Supporting Information for:

Direct Observation of Correlated Triplet Pair Dynamics During Singlet Fission Using Ultrafast Mid-IR Spectroscopy

Christopher Grieco[1], Eric R. Kennehan[1], Hwon Kim[2], Ryan D. Pensack[2], Alyssa N. Brigeman[3], Adam Rimshaw[1], Marcia M. Payne[4], John E. Anthony[4], Noel C. Giebink[3], Gregory D. Scholes[2], John B. Asbury[1*]

1. Department of Chemistry, The Pennsylvania State University
2. Department of Chemistry, Princeton University
3. Department of Electrical Engineering, The Pennsylvania State University
4. Department of Chemistry, University of Kentucky

Table of Contents:

S1. Fluorescence spectroscopy of TIPS-Pn solutions: Absence of excimer formation

The time-dependent fluorescence spectrum of a 0.2 mM TIPS-Pn solution (in CCl_4) was measured using 642 nm excitation. No appearance of excimer emission was observed in both spectral and kinetic data. In particular, no broad, lower energy emission features grew in over time, which is characteristic of excimer formation. The kinetic analysis provides further evidence against excimer formation since the kinetics at longer wavelengths matches exactly the kinetics at shorter wavelengths.

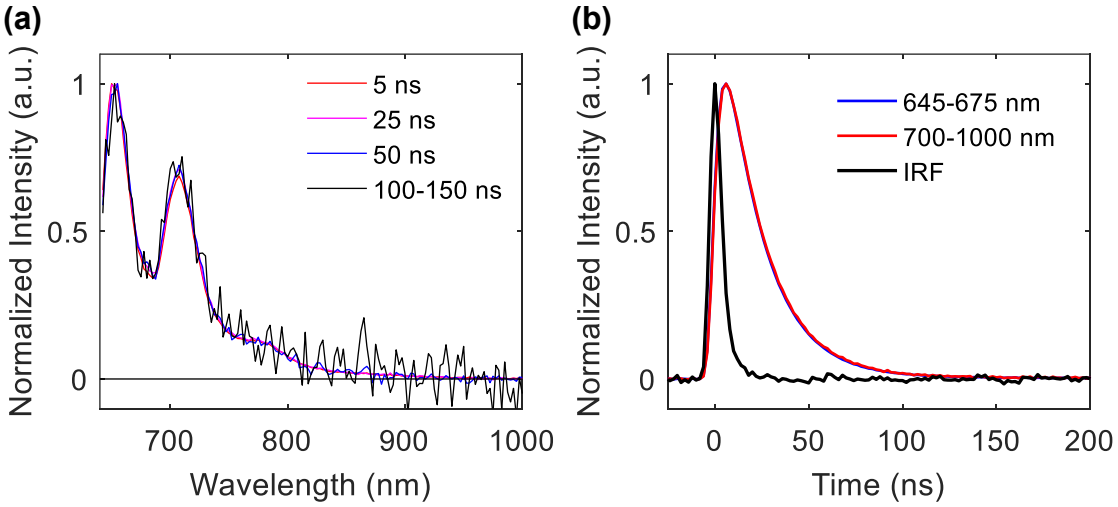

Figure S1. **(a)** Time-resolved fluorescence spectra of TIPS-Pn in a $2 \cdot 10^{-4}$ M CCl_4 solution. The fluorescence spectra do not change shape as a function of time, indicating the presence of only monomeric singlet excited states. **(b)** Corresponding kinetics integrated over short and long wavelength ranges showing no change in emission lifetime.

S2. Fluorescence spectra for TIPS-Pn in various solvents

The time-resolved fluorescence spectra were recorded for 0.2 mM TIPS-Pn solutions for a variety of solvents used in this study.

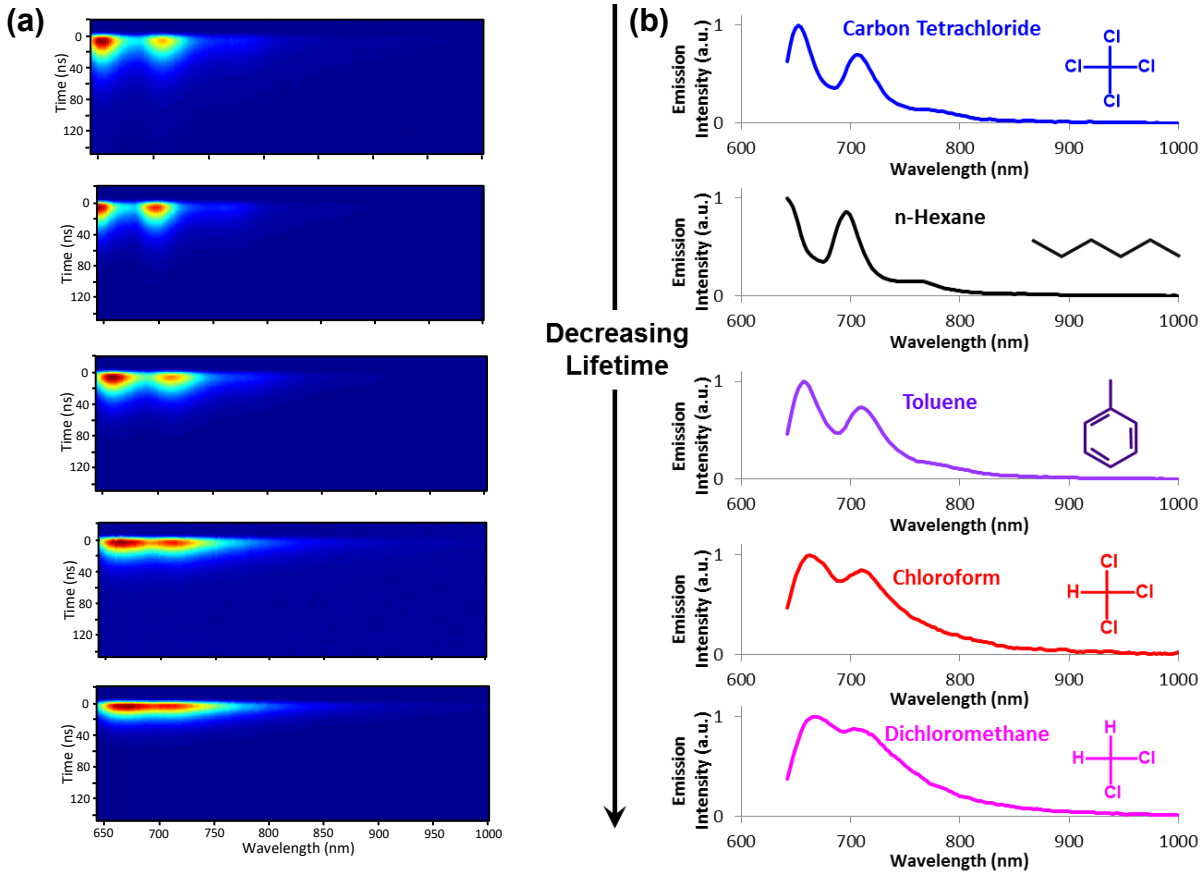

Figure S2. Fluorescence spectra for 0.2 mM TIPS-Pn solutions in a variety of solvents displayed as **(a)** contour plots and **(b)** 1D spectra. The spectra in **(b)** were produced by averaging the emission signal over time.

S3. Convolution fitting routine for mid-IR transient absorption and fluorescence decays

The kinetic decays of the mid-IR absorption feature as well as the fluorescence were measured for 0.2 mM solutions of TIPS-Pn in a variety of solvents. The instrument response was measured for each measurement technique, which was used to fit each kinetics trace in order to obtain accurate decay rate constants. The model, M(t), used to fit each kinetics trace was:

$$M(t) = F(t) * IRF(t) \quad \text{(eqn S1)}$$

$$F(t) = N * e^{-kt} \quad \text{(eqn S2)}$$

where t is time, IRF(t) is the instrument response function, F(t) is an exponential function describing the singlet excited state population, N is a normalization constant, and k is the first order (unimolecular) decay rate constant for the singlet excited state population. The results of all the fits are shown in **Figure S3**.

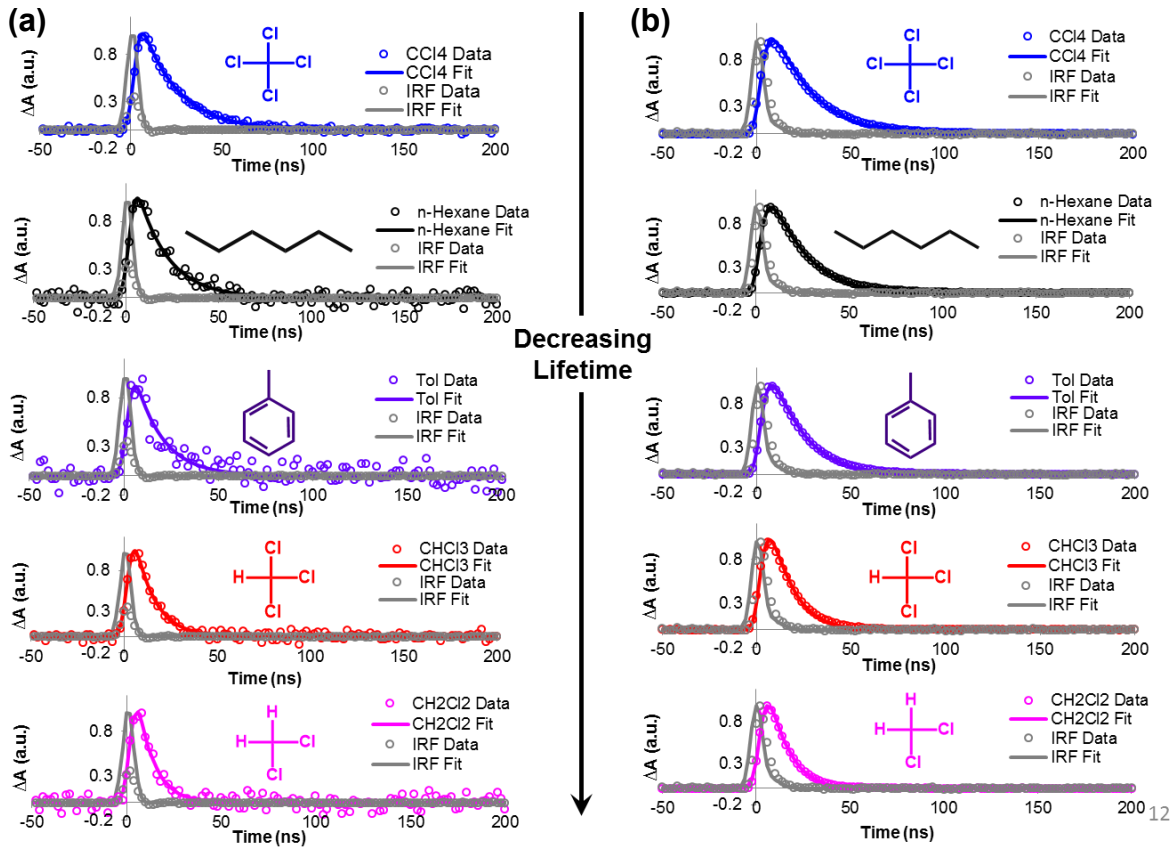

Figure S3. Kinetic decays of the singlet excited state population in 0.2 mM TIPS-Pn solutions probed either using **(a)** mid-IR transient absorption spectroscopy or **(b)** time-resolved photoluminescence spectroscopy. Data are provided as circles and solid colored lines are the fits to the data using an exponential decay model convoluted with each respective measurement's instrument response function (shown as gray). Solvents used are indicated in each plot.

The singlet decay rate constants were plotted against solvent polarity function[1] for reference, as shown in **Figure S4**.

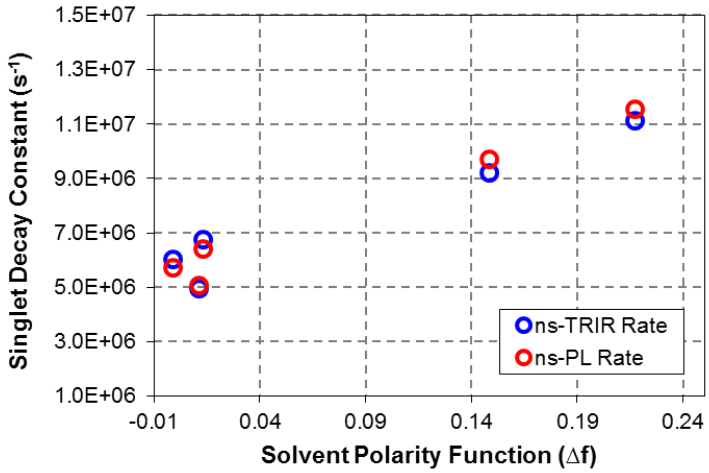

$$\Delta f = \left(\frac{\varepsilon - 1}{2\varepsilon + 1} - \frac{n^2 - 1}{2n^2 + 1} \right)$$

Figure S4. Singlet decay constants measured for 0.2 mM TIPS-Pn solutions using either nanosecond time-resolved IR (ns-TRIR) transient absorption spectroscopy or nanosecond time-resolved photoluminescence spectroscopy (ns-PL). Equation shows the solvent polarity function.

S4. Singlet excitations from steady-state absorbance spectra

The $S_0 \rightarrow S_3$ excitation energy was determined form a UV-Vis spectrum for a dilute solution of TIPS-Pn in toluene, as shown in **Figure S5**. The singlet excitation energies determined from steady state absorption spectroscopy are listed in **Table S1**.

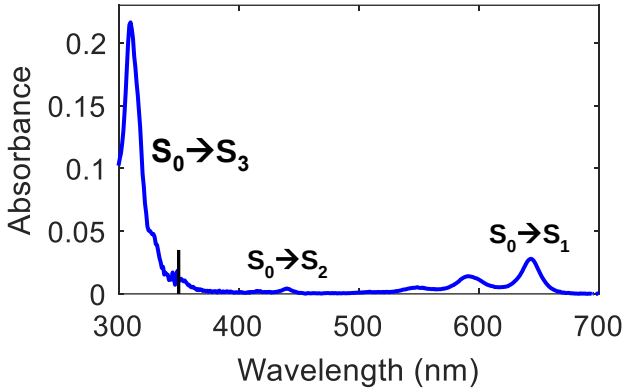

Figure S5. UV-Vis spectrum of a dilute solution of TIPS-Pn in toluene, showing the $S_0 \rightarrow S_3$ transition.

Table S1. Approximate excitation energies for dilute TIPS-Pn solution

Transition	Energy (ev)
$S_0 \rightarrow S_3$	3.543
$S_0 \rightarrow S_2$	2.818
$S_0 \rightarrow S_1$	1.925

S5. Excited state spectral assignments: Kinetics and molar extinction coefficients

Excited singlet and triplet state excitation spectra reported in the main text were identified by their characteristic decay kinetics: Single state absorption should decay on an early nanosecond timescale as does fluorescence; triplet state absorption should decay over longer timescales. In all our solution experiments, we relied on intersystem crossing (ISC) for the generation of triplet excited states. As such, the triplet state absorption should have a nanosecond rise component prior to its single exponential decay. All excitation spectra and their associated kinetics are provided in **Figure S6** below.

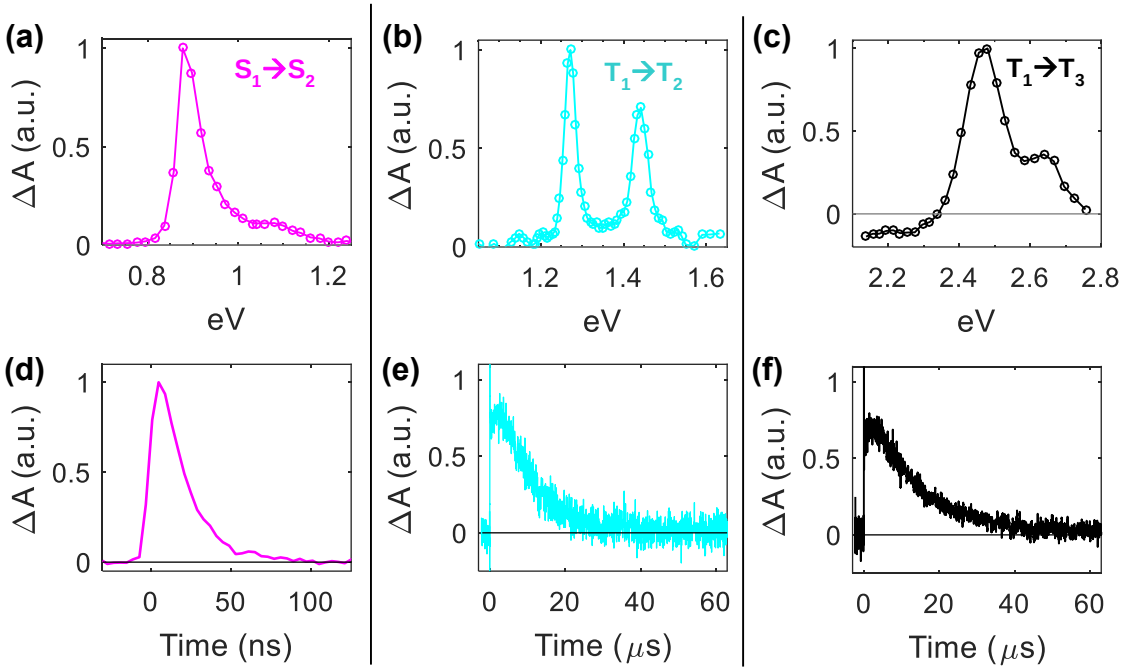

Figure S6. Excitation spectra for the **(a)** $S_1 \rightarrow S_2$, **(b)** $T_1 \rightarrow T_2$, and **(c)** $T_1 \rightarrow T_3$ transitions of TIPS-Pn in solution. The corresponding kinetic traces are provided in **(d)**, **(e)**, and **(f)**, respectively. Solvents used were either toluene or carbon tetrachloride. Solutions were purged of oxygen by bubbling N_2 gas prior to measurements.

These spectral data were combined to construct the experimental energy level diagram for the singlet and triplet manifolds that is represented in **Figure S7**. We note that the transition energy, 0.77 eV, for $S_0 \rightarrow T_n$ transition was taken from Reference 2. The states in the figure are labeled in accordance with the perimeter free electron orbital (PFEO) model[3] for pentacene.

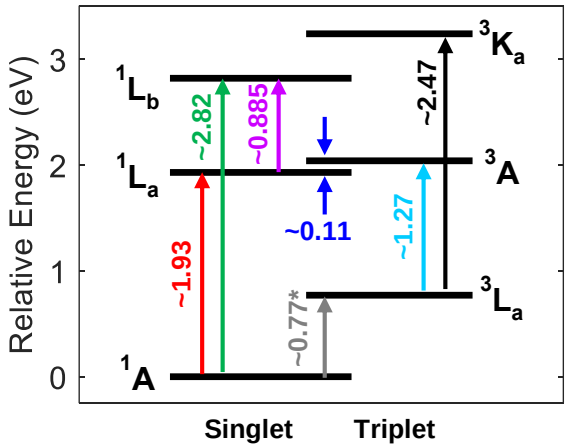

Figure S7. Energy level diagram for TIPS-Pn in solution based on the absorbance spectra represented in **Figure 3a**, including approximate transition energies. Both the singlet and triplet manifolds are represented. The states are described in accordance with the PFEO model for pentacene.

In order to estimate the extinction coefficient for each absorption feature, we first needed to calculate the initial excited state singlet concentration. We calculated this concentration as follows: First, we considered that the number of singlet excited states should be equal to the number of absorbed photons:

$$S_0 + h\nu \rightarrow S_1 \qquad \text{(eqn S3)}$$

where S_0 is the ground state singlet, and S_1 is the excited state singlet. From the experiment, the number of excited state molecules (n_{S1}) is:

$$n_{S_1} = n_{S_0} * (1 - 10^{-A_{642nm}}) \qquad \text{(eqn S4)}$$

where n_{S0} is the number of ground state molecules in the volume of excitation, and A_{624nm} is the absorbance of the sample at the excitation wavelength (642 nm). The initial number of singlet excited states was converted to concentration (c_{S1}) using Avogadro's constant (N_A) and the volume of the excitation spot (V_{ex}):

$$c_{S_1} = \frac{n_{S_1}}{N_A * V_{ex}} \quad \text{(eqn S5)}$$

To calculate the molar extinction coefficient (ε_λ) of a singlet state absorption we used Beer's Law as follows:

$$\varepsilon_\lambda = \frac{\Delta A_\lambda}{b * c_{S_1}} \quad \text{(eqn S6)}$$

where ΔA_λ is the initial transient absorption signal at probe wavelength, λ, and b is the pathlength. For the molar extinction coefficient values reported in the main text, we used the 0-0 vibronic peaks, and so λ was taken at the maximum absorption of the 0-0 band for each transition. In solution, the singlet population has not significantly decayed in the first few nanoseconds, and so we approximate the absorbance of the initial singlet excited state population as the kinetic signal at time zero.

To calculate the molar extinction coefficient for the triplet excited states, we needed to first calculate the initial triplet state concentration. Because we relied on ISC to generate the triplet population in the solutions, its initial concentration depends directly on quantum yield of ISC (Φ_{ISC}). We approximated this quantum yield based on a report of triplet generation of TIPS-Pn in chloroform solutions by Walker and coworkers.[4] We could therefore calculate the initial triplet concentration (c_{T1}) using:

$$c_{T_1} = c_{S_1} * \Phi_{ISC} \quad \text{(eqn S7)}$$

Once the initial triplet concentration was obtained, we could calculate its molar extinction coefficient using **equations S6**, except with parameter values now associated with the triplet state absorption.

S6. Determination of extinction coefficient of mid-IR transition in TIPS-Pn solutions

The extinction coefficient for the mid-IR singlet absorption was detetrmined by first measuring the absorption signal for solutions of TIPS-Pn having a variety of concentrations (**Figure S8a**). The absorption signal was taken as the average signal intensity across the first 25 ps time delays (before the singlet population has time to decay). Thus these signals correspond to the absorption of the initial singlet excited state population generated following photoexcitation. The concentration of the initial singlet excited state population was calculated in a manner similar to that described in **Section S5**. From Beer's law, plotting the transient absorption signal (ΔA) divided by the appropriate pathlength (b) against excited state concentration gives a linear relation where the slope is equal to the extinction coefficient (**Figure S8b**). We found the extinction coefficient at ~0.27 eV to be ~6.6 x 10^{-2} $M^{-1}cm^{-1}$.

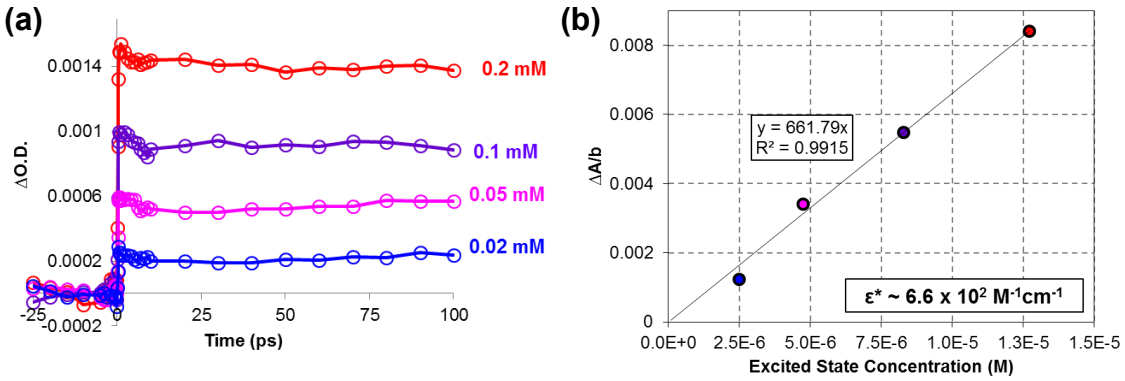

Figure S8. **(a)** Transient absorption kinetics of solutions of TIPS-Pn in CCl_4 for various concentrations probed at ~0.27 eV. **(b)** Dependence of the transient absorption signal in **(a)** on the excited state singlet concentration, revealing the extinction coefficient of the mid-IR absorption feature at ~0.27 eV.

S7. Assessing potential assignments of the mid-IR transition in TIPS-Pn solutions

An energy level diagram for TIPS-Pn in solution was constructed from absorbance and transient absorption measurements (see main text**).** Because we examined isolated molecules that did not electronically couple in their low concentration solutions, the possible assignments of the mid-IR transition cannot involve multiple chromophores. Therefore, we considered that the upper state involved in mid-IR transition might be a close lying singlet or triplet state.

Given the moderate oscillator strength of ~700 $M^{-1}cm^{-1}$, the most obvious possibility for the final state of the mid-IR transition is another singlet excited state ~0.2 eV higher in energy than the S_1 (^1L_a) state. Although the PFEO model does not predict states between the S_1 (^1L_a) and ^1L_b for pentacene (the putative S_2 state),[3] we considered that the alkynyl substituents of TIPS-pentacene could possibly introduce additional singlet excited states. To determine whether such additional states occur for TIPS-Pn, we performed density functional theory (DFT) computations to calculate the first few singlet excitation energies. We first optimized the geometry of the TIPS-Pn molecule in the calculation using the B3LYP functional, and then performed excitation energy calculations using time-dependent DFT (TD-DFT) with the B3LYP or the long-range corrected (LCR) wPBE functional (LCR-wPBE). All calculations were performed using the cc-PVTZ basis set,[5] and the polarized continuum model (PCM) for carbon tetrachloride. This approach was adapted from that performed for pentacene molecules as reported by Richard and Herbert, who explored how certain functionals are better for predicting certain singlet excitation energies than others.[6] The results of our calculations are provided in **Table S2**. Bolded values indicate the functionals that predicted excitation energies in good agreement with the experimental values and are consistent with the previous reports.[6-7] In all cases, no calculated singlet excitation energies

resulted in states falling in-between ^1L_a and ^1L_b, suggesting that the mid-IR absorption of TIPS-Pn solutions does not correspond to $S_1 \rightarrow S_n$.

Table S2: Calculated and experimental $S_1 \rightarrow S_n$ excitation energies of TIPS-Pn in eV

Final State	Experimental	LC-wPBE	B3LYP
S_4	-	4.1165	3.1119
S_3 (^1B_b)	3.54*	3.5351	3.0636
S_2 (^1L_b)	2.82	3.3591	**2.6617**
S_1 (^1L_a)	1.93	**2.0466**	1.6077

*See supporting information for determination of S_3 excitation energy

We considered it improbable that the mid-IR transition appearing in **Figure 2a** arose from a $S_1 \rightarrow T_n$ transition because transitions of this type are typically forbidden in organic molecules. We also considered the possibility that the mid-IR transition involved an intramolecular CT state[6] or intramolecular multi-exciton states[8-9]. It has been suggested in computational work by Richard and Herbert that the ^1L_a (S_1) state of pentacene may contain charge-separated character, with partial charges located on the ends of the pentacene molecule.[6] Zimmerman et al. suggested that initially excited S_1 states in pentacene dimers rapidly relax into multi-exciton D states that lie ~0.2 eV lower in energy than the S_1 state.[8-9] If such lower-lying, dark multi-exciton states are also present in TIPS-Pn, we do not believe they are accessed in dilute solutions because of the quantitative correspondence of the mid-IR and fluorescence decay rates. However, we considered the possibility that such states may lie slightly higher in energy, preventing molecules in the optically bright S_1 states in solution from relaxing into dark multi-exciton states.

To investigate the energies of multi-exciton states in TIPS-Pn, we used Complete Active Space Self Consisent Field (CASSCF) calculations performed at the B3LYP/6-31G(d)[10-11] level of theory optimized at the ground state and first excited bright state (S_1) geometries. All geometry optimization was performed with Gaussian09 Program.[12] All other calculations were performed with PySCF quantum chemistry package.[13] The CASSCF calculation was based on preliminary

calculation with Hartree-Fock with Dunning's triple-zeta basis[14] and was followed by Strongly Contracted N-electron Valence Perturbation Theory (SC-NEVPT) calculation[15] to account for the dynamic correlation. The results of these calculations along with the corresponding excitation energies and transition dipole moments are tabulated in **Table S3**. The excitation energy from ground state to the first bright state was obtained from the ground state S_0 geometry, and the excitation energy from the first bright state to doubly excited states was obtained from the S_1 state geometry. The active space incorporated 12 electrons and 12 orbitals, all of which were pi orbitals. The transition dipole was calculated from the CASSCF wavefunction, while the energy was calculated from NEVPT corrected energies of each state.

Table S3: Comparison of transition energies and oscillator strengths determined by calculation (for ethynyl-substituted pentacene) and by measurement (for TIPS-Pn).

	Oscillator Strength		Transition Energy (eV)	
Transition	**calc.**	**expt.**	**calc.**	**expt.**
S1->S2	0.006	0.034	0.67	0.885
S1->ME	0.011	0.0097	0.57	0.21
S0->S1	0.027	0.1565	1.79	1.93

The wavefunctions of the S_0, S_1, S_2 and ME states from CASSCF calculations were analyzed based on the weights of the configurations of the twelve CASSCF optimized orbitals. The three most important natural orbitals (NO) in the mutli-reference states computed from the CASSCF optimized orbitals are represented in **Figure S9**. **Table S4** tabulates the occupation of these NO in the four electronic states S_0, S_1, S_2 and ME. The NO1 and NO2 are nearly doubly occupied in S_0, with less than 0.5 occupation of NO3, and therefore the most dominant configuration is doubly occupied NO1 and NO2 with empty NO3. The S_1 state shows NO3 orbital occupied by one

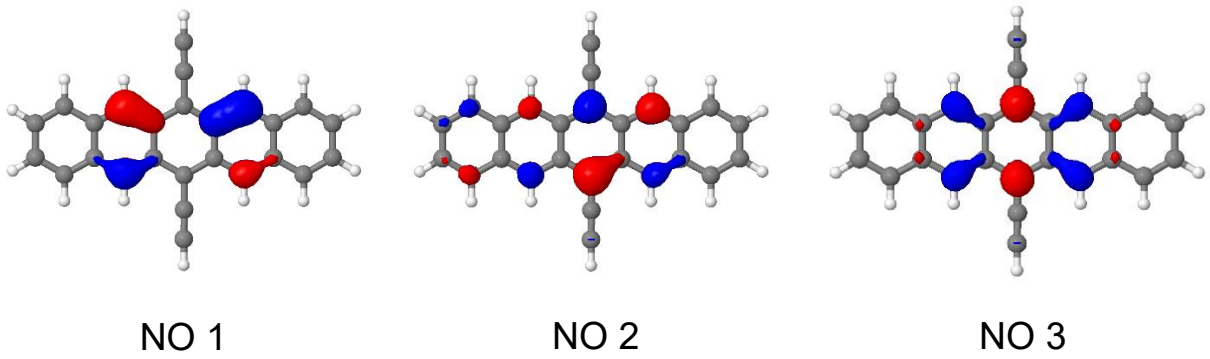

Figure S9. The three dominant natural orbitals (NO) computed from the CASSCF optimized orbitals of the TIPS-Pn model.

Table S4. Occupation numbers of each natural orbital (NO) obtained from CASSCF/NEVPT calculations of the first few electronic states of the TIPS-Pn model.

State	NO 1 Occupation Number	NO 2 Occupation Number	NO 3 Occupation Number
S_0	1.89	1.69	0.32
S_1	1.81	1.15	0.98
S_2	1.52	1.35	0.99
ME	1.71	0.66	1.42

electron and NO2 orbital occupied by one electron, showing the dominant transition is NO2 → NO3 for the $S_0 \rightarrow S_1$ electronic transition. The S_2 state shows significant reduction in occupancy of NO1 and NO2 with one electron occupying NO3, showing its multireference character. However, it is evident that NO1 → NO3 excitation takes place in the $S_0 \rightarrow S_2$ transition. The ME state shows occupation number of NO3 of 1.42 alongside the decrease of NO2 occupation number to 0.66. Even though the multireference character again makes the analysis elusive, the comparison of occupation numbers of S_1 state hints at the doubly excited character of ME state, as the ME state shows twice the decrease in occupation of NO2 and twice the increase in occupation of NO3.

As discussed in the context of Figure 3B in the main text, the ME state lies close in energy to the S1 state and has similar oscillator strength to the oscillator strength that is measured experimentally. Consequently, we assign the prompt mid-IR absorption to the S1 $\rightarrow$ ME electronic transition.

S8. Ultrafast fluorescence of amorphous TIPS-Pn films: The possibility of singlets that cannot undergo fission

To determine whether singlet excitons in amorphous TIPS-Pn films undergo bimolecular reformation (from triplet-triplet annihilation) or cannot undergo singlet fission and decay unimolecularly, we studied a "solid state solution" of TIPS-Pn in a polystyrene matrix. For making the film, we adopted a recipe reported in the past by Lukman and coworkers.[16] The absorbance spectrum (**Figure S10a**) of the TIPS-Pn/polystyrene film resembled that of a dilute TIPS-Pn/toluene solution, indicating that the molecules in the polystyrene film are isolated and do not electronically interact with other TIPS-Pn molecules. The fluorescence spectrum (**Figure S10b**) was found to not depend on excitation energy density over the range 3.8 – 382 $\mu J/cm^2$. The fluorescence kinetics (**Figure S10c**) had a single exponential decay time constant of ~12.5 ns, which is close to that of a dilute solution of TIPS-Pn in toluene (~15 ns). These observations confirmed that the TIPS-Pn molecules are isolated in the polystyrene matrix. Using this film as a control sample, we next measured the fluorescence of the amorphous TIPS-Pn film (**Figure S10d**). The shape of the spectrum resembled the TIPS-Pn/polystyrene spectrum, indicating that the fluorescence arises from monomeric-like singlet excitons. The fluorescence had a single exponential decay time constant of ~5.8 ns, which is close to that of the TIPS-Pn/polystyrene film. This time constant, combined with the unimolecular (single exponential) decay characteristic of the amorphous TIPS-Pn film, indicates that a population of singlet excitons forms in the film that cannot undergo singlet fission.

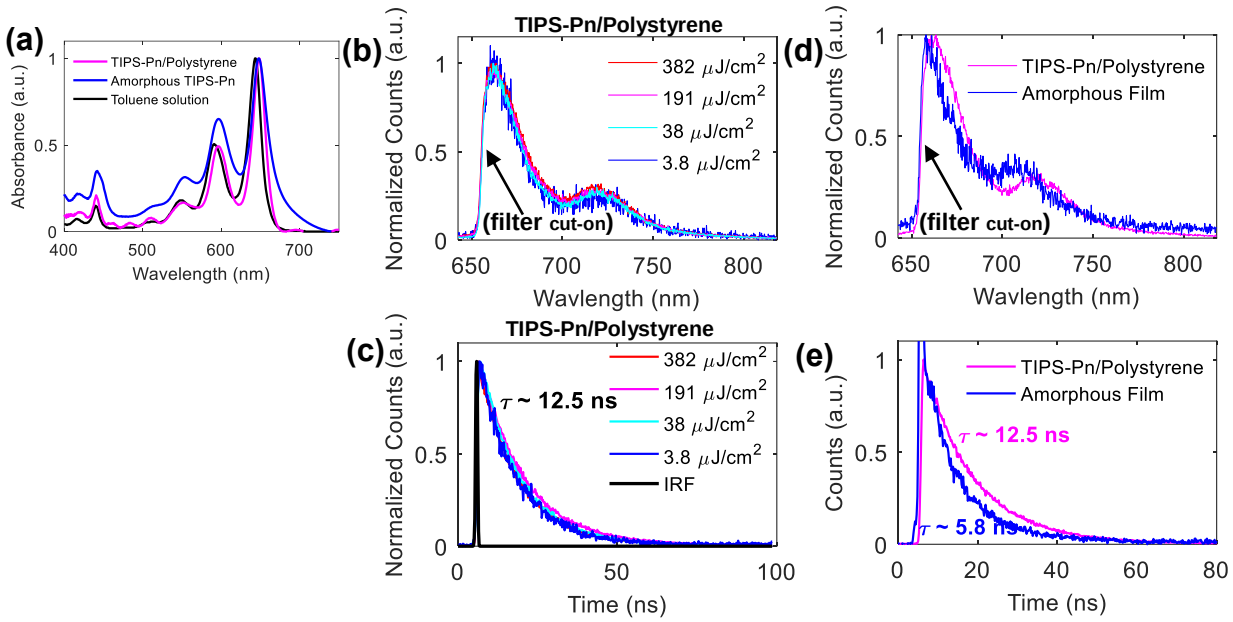

Figure S10. **(a)** Absorbance spectra for TIPS-Pn in various forms. **(b)** Fluorescence spectrum of a TIPS-Pn/polystyrene film measured using 633 nm excitation, showing no excitation energy density dependence. **(c)** Fluorescence decay kinetics for the TIPS-Pn/polystyrene film showing invariance over the excitation energy density range studied. The time constant from a single exponential fit to the data was ~12.5 ns, as indicated. **(d)** Comparison of the fluorescence spectrum for the amorphous TIPS-Pn film and the TIPS-Pn/polystyrene film, measured using 383 μJ/cm^2 excitation. **(e)** Fluorescence decay kinetics for the amorphous TIPS-Pn film compared to the TIPS-Pn/polystyrene film. The time constants from single exponential fits to the data are included.

S9. Bimolecular triplet decay kinetics and incident energy dependence

The triplet absorption kinetics for a crystalline TIPS-Pn film was measured across a range of incident excitation energy densities from ~5 – 280 μJ/cm^2. The decays were sensitive to energy density (**Figure S11a**) due to triplet-triplet annihilation. A plot of the absorption signal (taken at various delay times) against incident energy density (**Figure S11b**) provides quantitative evidence for triplet-triplet annihilation occurring on the ultrafast timescale for the excitation energy densities used in this work. The role of the triplet-triplet annihilation decay mechanism becomes particularly prominent at later time delays, even for the lowest excitation energy densities used.

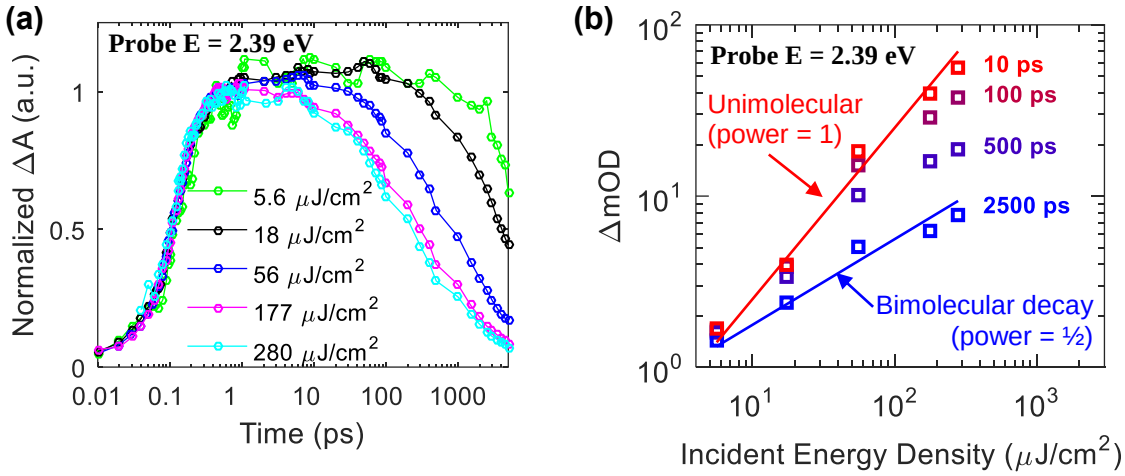

Figure S11: **(a)** Triplet absorption kinetics probed in the visible spectral region (2.39 eV) over a range of incident excitation energy densities. Decay shows excitation energy dependence, which is ascribable to triplet-triplet annihilation. **(b)** Dependence of the visible absorption signal on incident energy density, shown for several time delays. Linear and square-root functions (lines) are overlaid for reference.

S10. Rate equations for kinetic models of singlet fission

1-Intermediate state kinetic model:

We also considered the alternate (simpler) 1-intermediate state model commonly invoked in singlet fission reports. In accordance with Equation 1 of the main text, the coupled rate equations rate equations are therefore:

$$\frac{d[S_1S_2]}{dt} = -k_1[S_1S_0] + k_{-1}[\,^1(TT)] \quad \text{(eqn S8)}$$

$$\frac{d[\,^1(TT)]}{dt} = +k_1[S_1S_0] - k_{-1}\left[\,^1(TT)\right] - k_2\left[\,^1(TT)\right] + \frac{1}{2}k_{-2}[T_1]^2 \quad \text{(eqn S9)}$$

$$\frac{d[T_1]}{dt} = +2k_2\left[\,^1(TT)\right] - k_3[T_1]^2 - k_{-2}[T_1]^2 \quad \text{(eqn S10)}$$

To fit the kinetic data, we first solved these coupled rate equations numerically with the initial conditions: $[S_1S_0]_{t=0} = 1$; $[^1(TT)]_{t=0} = 0$; and $[T_1]_{t=0} = 0$. We then described the observed total kinetics using a linear combination of the kinetics of the appropriate absorbing species. Because absorption coefficients for all the states were not known, the normalized absorption kinetics were described using:

$$\frac{\Delta A_{mid-IR}(t)}{\Delta A_{mid-IR}^{max}} = a_1[S_1S_0](t) + a_2[\,^1(TT)](t) \quad \text{(eqn S11)}$$

$$\frac{\Delta A_{Vis}(t)}{\Delta A_{Vis}^{max}} = a_3[\,^1(TT)](t) + a_4[T_1](t) \quad \text{(eqn S12)}$$

where $\Delta A_{mid\text{-}IR}(t)$ is the change in absorbance for the mid-IR wavelength transition, $\Delta A_{Vis}(t)$ is the change in absorbance for the visible wavelength transition, a_i are scaling factors for each absorbing state.

2-Intermediate state kinetic model:

In accordance with **equation 2** of the main text, the coupled rate equations are therefore:

$$\frac{d[S_1S_0]}{dt} = -k_1[S_1S_0] \quad \text{(eqn S13)}$$

$$\frac{d[\,^1(TT)]}{dt} = +k_1[S_1S_0] - k_2\left[\,^1(TT)\right] \quad \text{(eqn S14)}$$

$$\frac{d[\,^1(T\ldots T)]}{dt} = +k_2\left[\,^1(TT)\right] - \frac{1}{2}k_3\left[\,^1(T\ldots T)\right] \quad \text{(eqn S15)}$$

$$\frac{d[T_1]}{dt} = +2k_3\left[\,^1(T\ldots T)\right] - \frac{1}{2}k_3[T_1]^2 \quad \text{(eqnS16)}$$

where $[S_1S_0]$ represents the concentration of singlet excitons, $[^1(TT)]$ represents the concentration of the proximal correlated triplet pair, $[^1(T\ldots T)]$ represents the concentration of the separated correlated triplet pair, $[T_1]$ represents the concentration of the thermalized triplet excitons, k_i are rate constants, and t is time.

The coupled rate equations derived from Equation 2 of the main text were solved numerically using the conditions: $[S_1S_0]_{t=0} = 1$; $[^1(TT)]_{t=0} = 0$; $[^1(T\ldots T)]_{t=0} = 0$; and $[T_1]_{t=0} = 0$. We then described the normalized observed kinetics using a linear combination of the kinetics of the appropriate absorbing species according to:

$$\frac{\Delta A_{mid-IR}(t)}{\Delta A_{mid-IR}^{max}} = a_1[S_1S_0](t) + a_2[\,^1(TT)](t) + a_3[\,^1(T\ldots T)](t) \quad \text{(eqnS17)}$$

$$\frac{\Delta A_{Vis}(t)}{\Delta A_{Vis}^{max}} = a_4[\,^1(TT)](t) + a_5[\,^1(T\ldots T)](t) + a_6[T_1](t) \quad \text{(eqnS18)}$$

where a_i are scaling factors for each absorbing state *i*, which are related to their absorption coefficients.

S11. One-state intermediate kinetic model

We investigated whether the mid-IR kinetic data could be described using the 1-intermediate state kinetic model (**equation 1** in main text). For convenience, this model is reproduced here:

$$S_1S_0 \overset{k_1}{\rightarrow} {}^1(TT) \overset{k_2}{\rightarrow} T_1 + T_1 \overset{k_3}{\rightarrow} S_0 + S_0 \qquad \text{(eqn S19)}$$

where S_1S_0 is the singlet exciton, ^{1}(TT) is the correlated triplet pair, and T_1 is a thermalized triplet exciton. We fixed the values of the rate constants, k_1 and k_2, obtained from visible absorption kinetic analysis of the triplet states.[17] The results of this model are shown in **Figure S12a**. We found that the mid-IR data were very poorly described under this model because the rate constant, k_2, was too fast to describe the mid-IR absorption beyond a few picoseconds.

We next considered whether the model could be improved by allowing k_2 to vary. The results of this approach are shown in **Figure S12b**. As observed in both the visible and mid-IR kinetic, the model fails to describe the curvature of the data.

Last, we considered turning on reverse reactions in the kinetic model. We found that turning on the reverse of k_1 trivially changed the initial decay of the model below 1 ps, having no effect on the data at later time delays. Next, we turned to the reverse of the second reaction step, characterized by k_2. In this case, correlated triplet pair reformation (reverse reaction of k_2) would occur at a rate constant of approximately 1/3 the rate of the forward reaction ($k_{2\text{-}} = 1/3*k_2$) .[18] The best fit under this kinetic model is shown in **Figure S12c**. We found that this model describes the data fairly well at later time delays, albeit the curvature in the data is not accurately reproduced by the model.

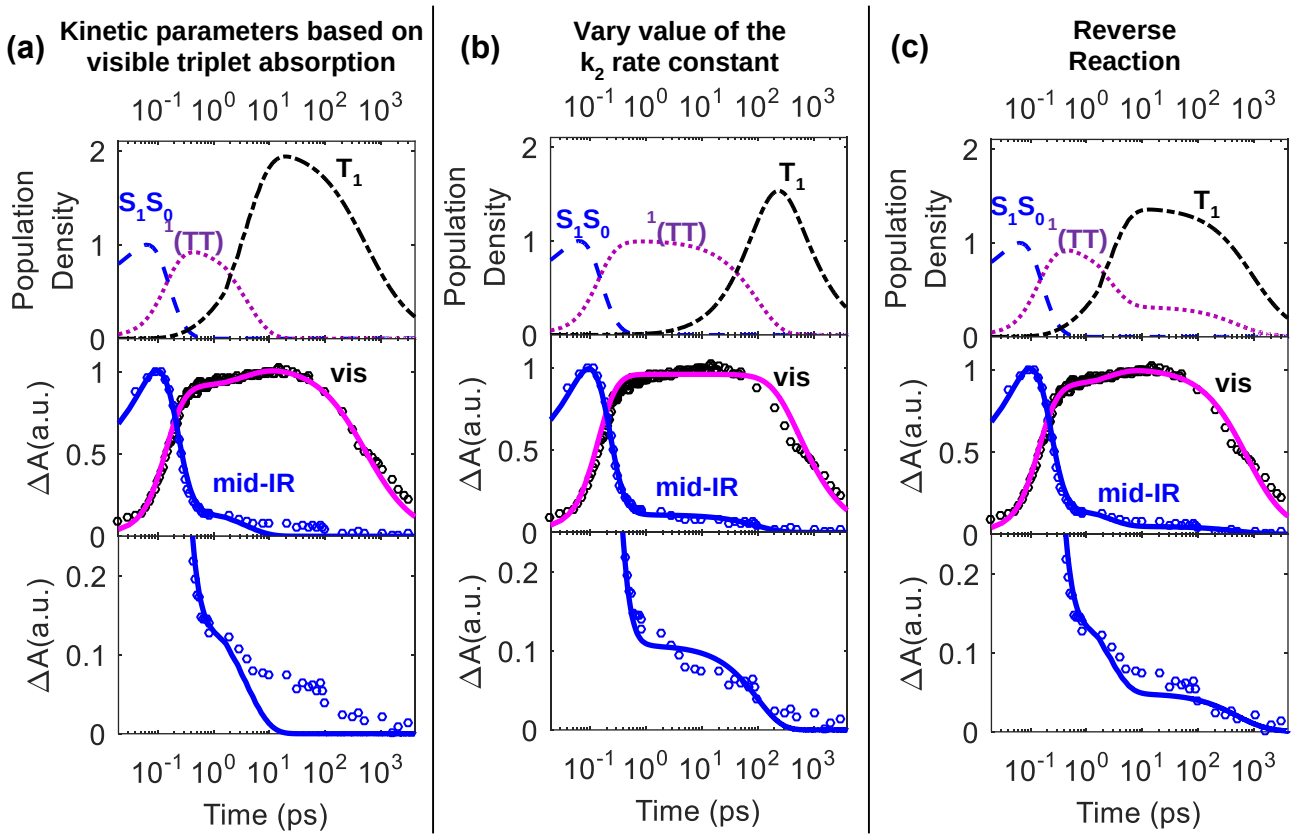

Figure S12: **(a)** Best fit of the 1-intermediate kinetic model to the mid-IR and visible transient absorption kinetics, using the values of the rate constant parameters obtained from visible absorption kinetic analysis. **(b)** Best fit of the 1-intermediate kinetic model when allowing k_2 to vary. **(c)** Best fit of the 1-intermediate kinetic model when allowing $k_{2\text{-}}$ (reverse of second reaction step) to vary. For all panels, data are shown as circles and kinetic models are shown as solid lines.

S12. Effect of reverse reactions on 2-intermediate state kinetic model

We investigated the effects of including reverse reactions for the 2-intermediate state kinetic model (**equation 2** in main text) for describing the mid-IR and visible transient absorption kinetics. For convenience, this model is reproduced here:

$$S_1S_0 \overset{k_1}{\rightarrow} {}^1(TT) \overset{k_2}{\rightarrow} {}^1(T\ldots T) \overset{k_3}{\rightarrow} T_1 + T_1 \overset{k_4}{\rightarrow} S_0 + S_0 \qquad \text{(eqn S20)}$$

where S_1S_0 is the singlet exciton, ^{1}(TT) is the proximal correlated triplet pair, ^{1}(T…T) is the distant correlated triplet pair, T_1 is a thermalized triplet exciton, and S_0 is the ground state. We fixed the values of the rate constants, k_1 and k_2, obtained from visible absorption kinetic analysis of the triplet states.[17] We demonstrated the effects of the reverse reactions by varying one reverse rate constant (k_{1-}, k_{2-}, or k_{3-}) at a time. In all cases, turning on the reverse reactions changes the yields of each reactive intermediate (as evidenced in the population density plots). As discussed in the main text, the absorption coefficients for each species is unknown, and so these parameters, a_i, must be varied in our case. As such, varying these parameters compensates for differences in the yields of each intermediate species, which are revealed by the population density output of the kinetic model (a trivial exception occurs when varying k_{1-}). Therefore, in all cases, the reverse reactions merely affect the apparent yields of each intermediate species, and do not significantly affect the rate constants obtained. Thus our conclusion in this work of long-lived intermediate states still holds true, although reverse reactions may indeed play roles in the singlet fission reaction.

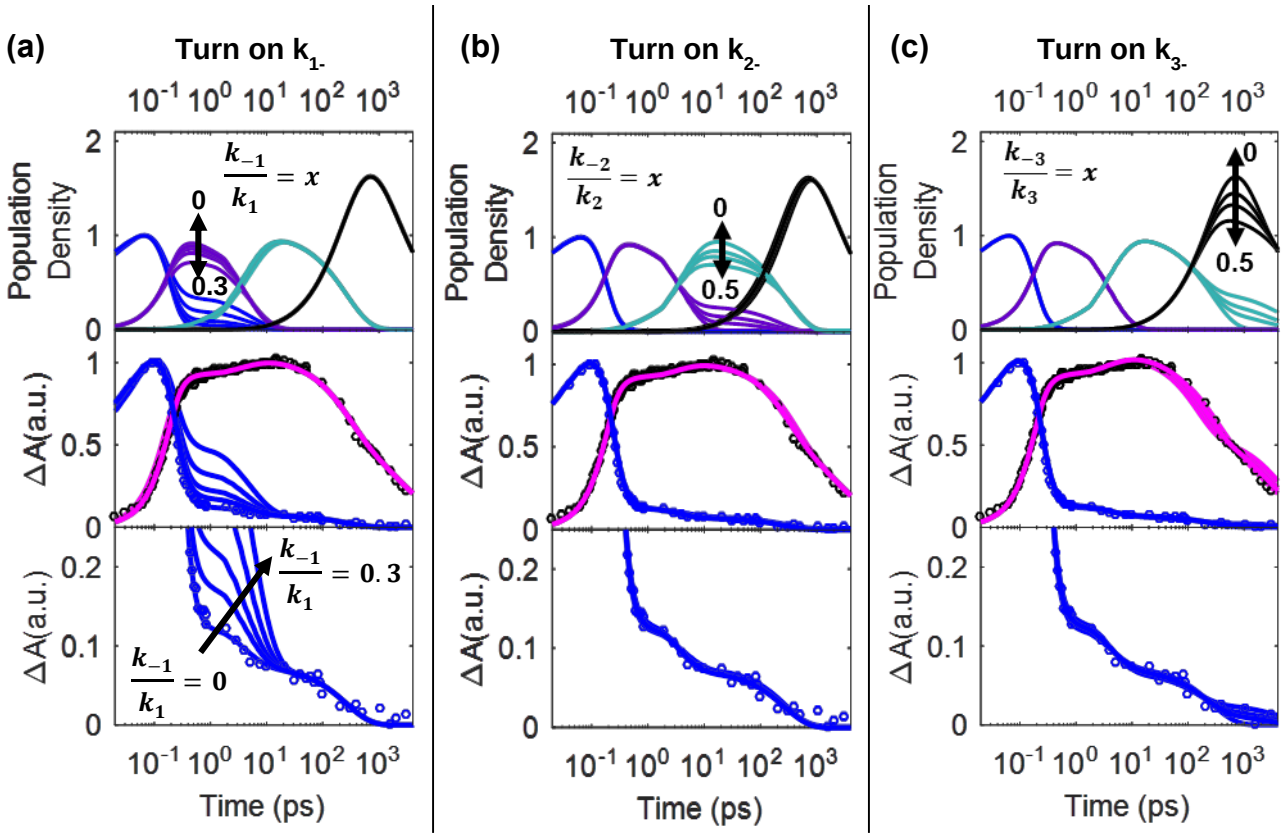

Figure S13: Effect of turning on reverse reactions on the best fits of the 2-intermediate kinetic model for **(a)** k_{1-}, **(b)** k_{2-}, and **(c)** k_{3-}. For all panels, data are shown as circles and kinetic models are shown as solid lines.

S13. Kinetic model results

The results of the 2-intermediate state kinetic modeling, one of the possibilities presented in the main text, are tabulated below in **Table S5** for reference.

Table S5. Parameters for the one CTP intermediate kinetic model for crystalline TIPS-Pn

Amplitude (a.u.)	Value	Rate Constant	Value (ps^{-1})
a_1	0.9670	k_1	12.5
a_2	0.1499	k_2	0.313
a_3	0.8925	$k_{-2} = 1/3\ k_2$	0.104
a_4	0.525	k_3	0.0028

Table S6. Parameters for the two CTP intermediate kinetic model for crystalline TIPS-Pn

Amplitude (a.u.)	Value	Rate Constant	Value (ps^{-1})
a_1	0.9809	k_1	12.5
a_2	0.1256	k_2	0.313
a_3	0.0724	k_3	0.0038
a_4	0.9039	k_4	0.0004
a_5	1.0180		
a_6	0.2506		

S14. References

1. Benniston, A. C.; Harriman, A.; Rostron, J. P., The effect of solvent polarity on the photophysical properties of 4-cyano-(4'-methylthio)diphenylacetylene: a prototypic donor-acceptor system. *Physical chemistry chemical physics : Phys. Chem. Chem. Phys.* **2005,** *7*, 3041-3047.
2. Zirzlmeier, J.; Lehnherr, D.; Coto, P. B.; Chernick, E. T.; Casillas, R.; Basel, B. S.; Thoss, M.; Tykwinski, R. R.; Guldi, D. M., Singlet fission in pentacene dimers. *Proc. Natl. Acad. Sci. U.S.A.* **2015,** *112*, 5325-5330.
3. Birks, J. B., Photophysics of Aromatic Molecules. *Ber. Bunseng. Phys. Chem.* **1970,** *74*, 1294-1295.
4. Walker, B. J.; Musser, A. J.; Beljonne, D.; Friend, R. H., Singlet exciton fission in solution. *Nat. Chem.* **2013,** *5*, 1019-1024.
5. Bogatko, S.; Haynes, P. D.; Sathian, J.; Wade, J.; Kim, J.-S.; Tan, K.-J.; Breeze, J.; Salvadori, E.; Horsfield, A.; Oxborrow, M., Molecular Design of a Room-Temperature Maser. *J. Phys. Chem. C* **2016,** *120*, 8251-8260.
6. Richard, R. M.; Herbert, J. M., Time-Dependent Density-Functional Description of the (1)La State in Polycyclic Aromatic Hydrocarbons: Charge-Transfer Character in Disguise? *J. Chem. Theory Comp.* **2011,** *7*, 1296-306.
7. Lopata, K.; Reslan, R.; Kowalska, M.; Neuhauser, D.; Govind, N.; Kowalski, K., Excited-State Studies of Polyacenes: A Comparative Picture Using EOMCCSD, CR-EOMCCSD(T), Range-Separated (LR/RT)-TDDFT, TD-PM3, and TD-ZINDO. *J. Chem. Theory Comp.* **2011,** *7*, 3686-93.
8. Zimmerman, P. M.; Bell, F.; Casanova, D.; Head-Gordon, M., Mechanism for singlet fission in pentacene and tetracene: from single exciton to two triplets. *J. Am. Chem. Soc.* **2011,** *133*, 19944-52.
9. Zimmerman, P. M.; Zhang, Z.; Musgrave, C. B., Singlet fission in pentacene through multi-exciton quantum states. *Nat. Chem.* **2010,** *2*, 648-52.
10. Lee, C.; Yang, W.; Parr, R. G., Development of the Colle-Salvetti Correlation-Energy Formula into a Functional of the Electron Density. *Phys. Rev. B* **1988,** *37*, 785-789.
11. Becke, A. D., Density-Functional Thermochemistry. III. The Role of Exact Exchange. *J. Chem. Phys.* **1993,** *98*, 5648-5652.
12. Gaussian 09, R. E., Frisch, M. J.; Trucks, G. W.; Schlegel, H. B.; Scuseria, G. E.; Robb, M. A.; Cheeseman, J. R.; Scalmani, G.; Barone, V.; Mennucci, B.; Petersson, G. A.; Nakatsuji, H.; Caricato, M.; Li, X.; Hratchian, H. P.; Izmaylov, A. F.; Bloino, J.; Zheng, G.; Sonnenberg, J. L.; Hada, M.; Ehara, M.; Toyota, K.; Fukuda, R.; Hasegawa, J.; Ishida, M.; Nakajima, T.; Honda, Y.; Kitao, O.; Nakai, H.; Vreven, T.; Montgomery, J. A., Jr.; Peralta, J. E.; Ogliaro, F.; Bearpark, M.; Heyd, J. J.; Brothers, E.; Kudin, K. N.; Staroverov, V. N.; Kobayashi, R.; Normand, J.; Raghavachari, K.; Rendell, A.; Burant, J. C.; Iyengar, S. S.; Tomasi, J.; Cossi, M.; Rega, N.; Millam, J. M.; Klene, M.; Knox, J. E.; Cross, J. B.; Bakken, V.; Adamo, C.; Jaramillo, J.; Gomperts, R.; Stratmann, R. E.; Yazyev, O.; Austin, A. J.; Cammi, R.; Pomelli, C.; Ochterski, J. W.; Martin, R. L.; Morokuma, K.; Zakrzewski, V. G.; Voth, G. A.; Salvador, P.; Dannenberg, J. J.; Dapprich, S.; Daniels, A. D.; Farkas, Ö.; Foresman, J. B.; Ortiz, J. V.; Cioslowski, J.; Fox, D. J. Gaussian, Inc., Wallingford CT, 2009.

13. Sun, Q.; Berkelbach, T. C.; Blunt, N. S.; Booth, G. H.; Guo, S.; Li, Z.; Liu, J.; McClain, J. D.; Sayfutyarova, E. R.; Sharma, S.; Wouters, S.; Chan, G. K.-L. PySCF: The Python-based Simulations of Chemistry Framework 2017. http://arxiv.org/abs/1701.08223 (accessed August 2017).
14. Dunning, T. H. J., Gaussian Basis Sets for Use in Correlated Molecular Calculations. I. The Atoms Boron through Neon and Hydrogen. *J. Chem. Phys.* **1989,** *90*, 1007-1023.
15. Angeli, C.; Cimiraglia, R.; Evangelisti, S.; Leininger, T.; Malrieu, J.-P., Introduction of N-Electron Valence States for Multireference Perturbation Theory. *J. Chem. Phys.* **2001,** *114*, 10252-10264.
16. Lukman, S.; Musser, A. J.; Chen, K.; Athanasopoulos, S.; Yong, C. K.; Zeng, Z.; Ye, Q.; Chi, C.; Hodgkiss, J. M.; Wu, J.; Friend, R. H.; Greenham, N. C., Tuneable Singlet Exciton Fission and Triplet-Triplet Annihilation in an Orthogonal Pentacene Dimer. *Adv. Funct. Mater.* **2015,** *25*, 5452-5461.
17. Pensack, R. D.; Tilley, A. J.; Parkin, S. R.; Lee, T. S.; Payne, M. M.; Gao, D.; Jahnke, A. A.; Oblinsky, D. G.; Li, P. F.; Anthony, J. E.; Seferos, D. S.; Scholes, G. D., Exciton delocalization drives rapid singlet fission in nanoparticles of acene derivatives. *J. Am. Chem. Soc.* **2015,** *137*, 6790-803.
18. Scholes, G. D., Correlated Pair States Formed by Singlet Fission and Exciton-Exciton Annihilation. *J. Phys. Chem. A* **2015,** *119*, 12699-12705.